Total Column Ozone Trends from the NASA Merged Ozone Time Series 1979 to 2021 Showing Latitude Dependent Ozone Recovery Dates (1994 to 1998)

Jay Herman[1], Jerald Ziemke[2], and Richard McPeters[3]

Changes in response to Reviewer 1 are marked in Green.

Changes in response to Reviewer 2 are marked in Yellow.

Changes in response to Reviewer 2 are marked in Grey

Changes by the author are also marked in Green.

[1]University of Maryland Baltimore County, Baltimore Maryland USA

[2]Morgan State University, Baltimore Maryland, USA

[3]NASA Goddard Space Flight Center, Greenbelt, Maryland, USA

Corresponding Author: Jay Herman Herman@umbc.edu

Abstract

Monthly averaged total column ozone data $\Omega_{MOD}(t,\theta)$ from the NASA Merged Ozone Data set (MOD) were examined to show that the latitude-dependent, θ, ozone depletion turnaround dates $T_A(\theta)$ range from 1994 to 1998. $T_A(\theta)$ is defined as the approximate date when the zonally average ozone ceased decreasing. Ω_{MOD} data used in this study were created by combining data from Solar Backscattered Ultraviolet instruments (SBUV/SBUV-2) and the Ozone Mapping and Profiler Suite (OMPS-NP) from 1979 to 2021. The new calculated systematic latitude-dependent hemispherically asymmetric $T_A(\theta)$ shape should appear in atmospheric models that combine the effects of photochemistry, volcanic eruptions, and dynamics in their estimate of ozone recovery. Trends of zonally averaged total column ozone in percent per decade were computed before and after $T_A(\theta)$ using two different trend estimate methods that closely agree, Fourier Series Multivariate Linear Regression and linear regression on annual averages. During the period 1979 to $T_A(\theta)$ the most dramatic rates of SH ozone loss were P_D = -10.9 ± 3 % per decade at 77.5^{O}S and -8.5±0.9% per decade at 65^{O}S, which is about double the NH rate of loss of P_D = -5.6±4 %/decade at 77.5^{O}N and 4.4±1%/decade at 65^{O}N for the period 1979 to $T_A(\theta)$. After $T_A(\theta)$, there has been an increase at 65^{O}S of P_D = 1.6±1.4% per decade with smaller increases from 55^{O}S to 25^{O}S and a small decrease at 35^{O}N of -0.4±0.3 %/decade. Except for the Antarctic region, there only has been a small recovery in the Southern Hemisphere toward 1979 ozone values and almost none in the Northern Hemisphere.

1.0 Introduction

Ozone is a photolytically produced, photochemically destroyed, and dynamically distributed atmospheric gas that plays a crucial role in protecting the planet from harmful ultraviolet (UV) radiation from the sun. The atmospheric presence of bromine and the release of chlorine from the UV dissociation of man-made chemicals, such as chlorofluorocarbons (CFCs), can break down the ozone layer at all latitudes. This is especially the case in the Antarctic region where heterogeneous chemistry on and within ice crystals and liquid droplets (Tritscher, et al., 2021) in polar stratospheric clouds PSCs have a strong effect on the destruction of ozone during September and October (WMO, 2022; Tritscher, et al., 2021; Solomon et al., 1986; 1999; 2016; Crutzen and Arnold, 1986; Khosrawi et al., 2011). As the sun rises in Spring, chemically active nitrogen oxides, chlorine and bromine are released causing the ozone hole to develop within the region enclosed by the polar vortex winds. The weak levels of sunlight are sufficient to initiate and maintain the catalytic ozone loss photochemistry. In November and December, the isolating polar vortex winds break down and the Antarctic ozone hole region back fills by air exchange from southern mid-latitudes causing $T_A(35^OS – 65^OS)$ to be delayed compared to the Northern Hemisphere NH mid-latitudes. The recurring annual ozone hole event triggered international action to limit the production and use of ozone-depleting substances (ODS) under the Montreal Protocol, which has been successful in reducing the emission of these substances, slowing down the depletion of the ozone layer globally, leading to a partial recovery in the Antarctic ozone hole region (Solomon et al., 2016; Strahan and Douglass 2018). After the mid-1990s, several studies have reported an increase in total column ozone (TCO), particularly in the mid to high latitudes of the Southern Hemisphere, as well as a reduction in the size and depth of the Antarctic ozone hole starting in the late 1990s (Solomon et al., 2016; Stone et al., 2018; 2021, Weber et al., 2022).

The cessation of ozone decrease was first observed in the mid-1990s when satellite data showed a stabilization and slight increase in ozone concentrations in the Antarctic ozone hole region. However, the recovery was not significant enough to be considered a trend at that time (Strahan and Douglass 2018). In the early 2000s, further analysis of satellite and ground-based data showed that the rate of ozone depletion had slowed down. After the mid-1990's, the cessation of ozone depletion has been most evident in the Southern Hemisphere SH polar region, where ozone depletion had been most severe. Ozone recovery has been slow or non-existent at other latitudes. Recently, Weber et al. (2022) showed reduction in ozone at all latitudes prior to 1995 and reported positive statistically significant TCO trends from 1996-2020 at southern middle and high latitudes, and over the SH polar cap in September. When dynamical terms were included in the regression, small positive trends were near the 2-standard deviation 2σ threshold at northern mid- and high-latitudes, with no trend detected in the tropics or over the NH polar cap.

Despite the success of the Montreal Protocol (Velders and Andersen, 2018), ozone concentrations continue to fluctuate, driven by natural and anthropogenic factors, such as, changes in solar radiation, stratospheric circulation, global warming, volcanic activity, and changing emissions of ozone precursors (Dameris and Baldwin, 2012; Weber et al., 2022). The discussion by Dameris and Baldwin (2012) explored possible effects of climate change on the dynamics of the atmosphere affecting ozone as ODSs change, and particularly the change in the Brewer-Dobson circulation (Brewer, 1949; Dobson et al.,

1926) that transports ozone from an upwelling in the equatorial region into the stratosphere and to downwelling into mid- and high-latitudes.

This study will estimate new latitude dependent ozone recovery dates, or more accurately the dates of cessation of ozone decrease, $T_A(\theta)$ ranging from 1994 (equatorial region and 60^ON to 70^ON) to 1998 (60^OS – 80^OS). The calculated $T_A(\theta)$ and ozone trends (%/decade) include the effects of volcanic eruptions such as Mt. Pinatubo in 1991, dynamics, and atmospheric temperature changes. Ozone data used in this study are a subset of the Merged Ozone Data MOD set $\Omega_{MOD}(t)$ (1970 – 2021) starting in 1979 with the Nimbus-7 SBUV (Solar Backscattered Ultraviolet) satellite instrument. From 1979 to 2021, the MOD data set was created by combining data from Solar Backscattered Ultraviolet instruments (SBUV/SBUV-2) and the Ozone Mapping and Profiler Suite (OMPS-NP). Methods of calculating trends from time series data are essential in the analysis of environmental and climate-related data. Here, we discuss two independent methods to estimate linear trends: 1) linear regression of annual averaged data and 2) Fourier time series decomposition or multivariate linear regression MLR (Ziemke et al., 2019) are discussed below. The two methods are compared and shown to give nearly identical results over their mutual latitude range of validity, 65^OS to 65^ON. The MLR method is not used in the regions poleward of the Arctic and Antarctic circles that have latitude dependent extended winter polar night. The advantage of the MLR method (Eq. 1), or that in Weber et al, 2002, is that it can be used to estimate the effects of its individual components, while the annual average method can be used in the polar regions where there is latitude dependent extended winter night.

1.1 The Merged Ozone Data Set MOD

Figure 1 (left panel) shows the MOD zonally averaged Ω_{MOD} TCO data (Frith et al., 2014; 2020) set as a function of latitude (5^O latitude bands from 77.5^OS to 77.5^ON) and time (January 1979 to December 2021). Part of the Antarctic ozone hole (75^OS to 80^OS) is shown (blue color), and the high latitude maxima, North and South, (red color), with low values in the equatorial region. Figure 1 (right panel) shows the 42-year zonal and time averaged ozone amounts and the maxima and minima annual envelopes as a function of latitude. Figure 1 shows the asymmetry in the monthly and zonally averaged ozone data between the hemispheres, with the Northern Hemisphere NH having more ozone than the Southern Hemisphere SH at corresponding latitudes. Part of the asymmetry is driven by the Spring Antarctic ozone hole backfilling in the SH summer.

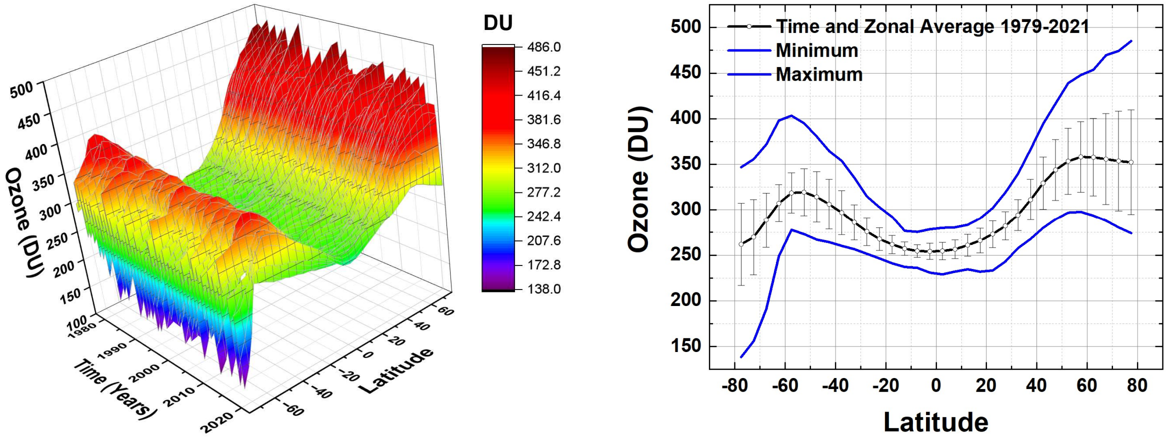

Fig. 1 Left: The zonally and monthly averaged Ω_{MOD} data set 1979 – 2021 and -77.5^O to 77.5^O. Right: Time and zonal averaged ozone and its maxima and minima 1979 – 2021. Error bars are 1 standard deviation $\pm 1\sigma$.

$\Omega_{MOD}(t,\theta)$ provides a global view of ozone levels needed to track changes in ozone concentrations over time t for each latitude band θ. The SBUV and OMPS-NP series of satellite instruments form the longest (1979 to 2022) continuous global ozone $\Omega_{MOD}(t,\theta)$ data record from a single instrument type. Merged ozone retrievals from the individual instruments use the version 8.7 retrieval algorithm (described by Weber et al., 2022) as an extension of the version 8.6 algorithm (Bhartia et al., 2013; McPeters et al., 2013; DeLand et al., 2012; Frith et al., 2017) specifically designed to improve cross calibrations between the later SBUV-type instruments in MOD starting from NOAA-16 in 2000. There were no external adjustments made to the ozone retrieval except for small high-altitude (> 35 km) diurnal corrections to account for different measurement times between satellites and varying measurement time of day as individual satellite orbits slowly drift in equator crossing time. These adjustments are very minor in TCO (Frith, personal communication). Data from each instrument are selected based on quality criteria outlined in Frith et al. (2014; 2020) and the data are averaged during periods when more than one instrument was operational. The $\Omega_{MOD}(t,\theta)$ are available as a function of latitude and month, [https://acd-ext.gsfc.nasa.gov/Data_services/merged/.](https://acd-ext.gsfc.nasa.gov/Data_services/merged/)

Analysis of the long-term ozone time series has been looked at extensively with references given in Weber et al., 2022. Methods for estimating trends from an oscillating time series with several distinct periodicities are well known (Ziemke et al., 2019; Stolarski et al. 1991;1992, Herman et al., 1993). For ozone, one of the difficulties in trend estimation is that the early part of the time series shows a strong ozone decrease at all latitudes that continued until the mid-1990s and then flattens out and shows almost no recovery thereafter toward 1979 values. The Ω_{MOD} time series has been used extensively in ozone assessments and State of the Climate reports (e.g., WMO, 2022) and was recently compared to several other merged total ozone records in Weber et al. (2022). The validity of the Ω_{MOD} time series for estimating ozone trends was further checked (See Appendix Figs. A1 to A3) in this study by showing detailed comparisons between the deseasonalized Ω_{MOD} time series with the deseasonalized MLS (Microwave Limb Sounder) overlapping stratospheric ozone time series (2005 to 2023).

2.0 Trend Estimates from the MOD Ozone Data

Multivariate Linear Regression MLR is a Fourier based method for analyzing atmospheric time series data that decomposes the time series into its component parts, including trend, quasi-biennial oscillation QBO, solar cycle, ENSO (El Nino Southern Oscillation), seasonality, and noise resulting in a trend estimate and 2-standard deviation 2σ uncertainty estimates (Ziemke et al., 2019). Calculated 2σ uncertainties for the MLR trends include a first order autoregressive adjustment applied to the derived residuals (Weatherhead et al., 1998).

Linear trend estimates for the long-term changes in $\Omega_{MOD}(t, \theta_i)$ globally and as a function of latitude θ_i have been obtained using the multivariate linear regression (MLR) model (e.g., Randel and Cobb, 1994, and references therein). Trends $B(\theta_i)$ were determined for $\Omega_{MOD}(t, \theta_i)$ using Eqns. 1 and 2.

$$\Omega_{MOD}(t, \theta_i) = A(\theta_l\ t) + B(\theta_l,t)\cdot t + C(\theta_l,t)\cdot QBO_1(t) + D(\theta_l,t)\cdot QBO_2(t) + E(\theta_l,t)\cdot ENSO(t) + F(\theta_l,t)\cdot Solar(t) + R(t, \theta_l) \qquad (1)$$

where t is the month index (t=1 to 516 months with data for 1979–2021), $A(\theta_i\ t)$ is the seasonal cycle coefficient, $B(\theta_i,t)$ is the trend coefficient, $C(\theta_l,t)$ is the first empirical orthogonal function (EOF) QBO coefficient, $D(\theta_l,t)$ is the second EOF QBO coefficient, both representing the major components of the QBO variability, $E(\theta_l,t)$ is the ENSO coefficient, $F(\theta_l,t)$ is the solar cycle coefficient, and R(t) is the residual error time series. The F10.7 cm solar flux monthly time series is used for the Solar(t) proxy, first and second leading EOF QBO monthly time series proxies $QBO_1(t)$ and $QBO_2(t)$ are used for the QBO component (Wallace et al., 1993), and Nino 3.4 (Oldenborgh *et al* 2021) is used for ENSO(t) (Nino 3.4: https://www.ncei.noaa.gov/access/monitoring/enso/sst). $QBO_1(t)$ and $QBO_2(t)$ are nearly orthogonal (correlation coefficient approximately zero) oscillating time series based on data with approximately a 2.3-year periodicity. $A(\theta_l,t)$ involves 7 fixed constants while $B(\theta_l,t)$ (and all other remaining coefficients) involves 5 fixed constants for each θ_l. The harmonic expansion for A(t) (similar for the other coefficients) is (Eqn. 2).

$$A(t) = a(0) + \sum_{p=1}^{3}\left[a(p)\cos(2\pi pt/365) + b(p)\sin(2\pi pt/365)\right] \qquad (2)$$

where a(p) and b(p) are constants. Statistical uncertainties for A(t) and $B(\theta_i)$ were derived from the calculated statistical covariance matrix involving the variances and cross-covariances of the constants (e.g., Guttman et al., 1982; Randel and Cobb, 1994).

In this study the Locally Weighted Scatterplot Smoothing Lowess(f) least-squares technique is used to reduce oscillations in the time series data and to estimate $T_A(\theta)$where f = the fraction of data averaged together (Cleveland, 1979 and Cleveland and Devlin, 1988).

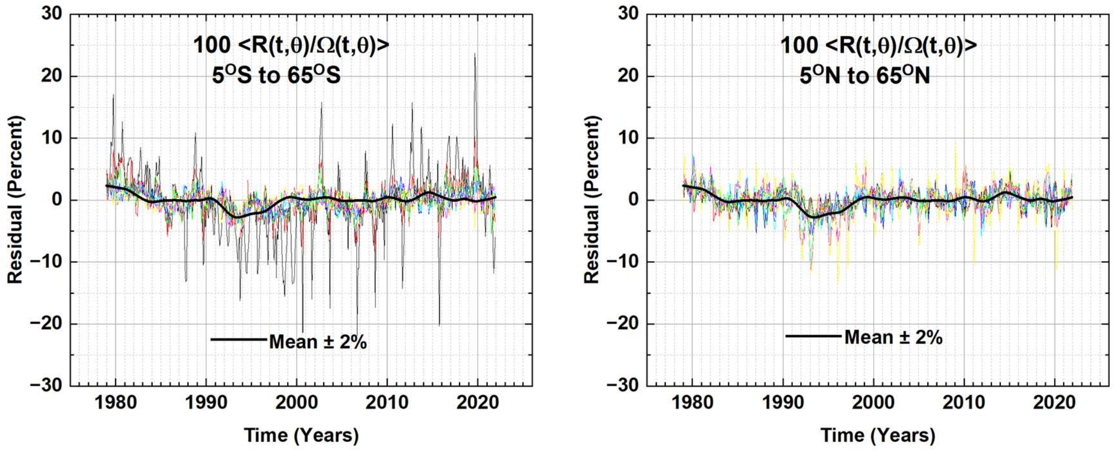

Fig. 2 The latitude average residual term from Eq. 1 in percent $100 <R(t,q_i)/W_{MOD}(t,q_i)>$ The black line is the Lowess(0.1) fit (Cleveland, 1979) to the R(t,q) with an average error estimate of ±2%. The light-colored lines are each latitude's R(t,q) in a hemisphere $0^O < \theta < 65^O$.

The latitude average residual R(t) in percent of the MOD ozone amount ($100 <R(t,\theta_i)/ \Omega_{MOD}(t,\theta_i)>$) is shown in Fig. 2 for the SH and NH as an indication of how well Eq 1 is able to fit the $\Omega_{MOD}(t,\theta_i)$ time series.

The SH $R(t,\theta)$ is more variable than the NH with the largest variations arising in the 55^OS and 65^OS latitude bands. On average Eq. 1 fits the original data $\Omega_{MOD}(t,\theta_i)$ to within ±2%.

The linear deseasonalized trend results $B(\theta_i)$ are obtained for 14 latitude bands θ_i (centered on 65^OS to 65^ON). The latitudinal trends $P_D(\theta_i)$ are expressed in %/Decade given by Eq. 3, where the denominator D is either the time average $<\Omega>$ of the area weighted global ozone average (Fig 1) or the time average $D(\theta_i) = < \Omega_{MOD}(t, \theta_i)>$ for each latitude band over the considered period. The whole year period considered is 1979 – 2021.

$$P_D(\theta_i) = 1000\ B(\theta_i)\ /D(\theta_i) \qquad (\%\ /\ \text{Decade}) \tag{3}$$

In the second method, the trend is estimated using annual integrals (annual averages) that remove the seasonality and other short-term oscillations but ignore longer term oscillations such as the 28-to-29-month QBO cycle and the average 11.3-year solar cycle. A comparison of the two trend estimating methods is shown in Fig. 3 for the entire 1979 to 2021 period showing that they agree quite closely, but that the annual average method has slightly larger two standard deviations 2σ than the MLR method.

The MLR method (Eqns. 1 and 2) are not applied poleward of the Arctic and Antarctic circles where latitude dependent extended winter night periods occur**.** Additional latitude dependent terms of varying periods would be needed for latitudes greater than 70^O. The annual average method does not have these complications.

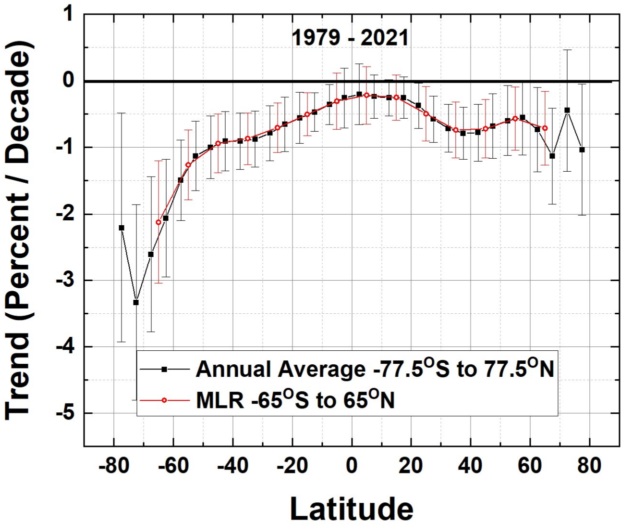

Fig. 3 The ozone trend $P_D(\theta)$ for the entire period 1979 – 2021 for two methods, MLR and Annual Average. The latitude grids for the two methods are offset to show the agreement in the trends and 2σ error bars.

The Fig. 3 estimation of linear long-term trends since 1979 is misleading, since ozone showed significant annual declines until the mid-1990s and then increased slightly thereafter, meaning the average long-term time series is non-linear. The usual procedure is to determine linear trends separately before and after the turnaround dates T_A (Weber et al., 2022). However, as is shown later, there is no single turnaround date applicable to all the latitudes between 80°S and 80°N. Instead, there is a range spanning 1994 to 1998.

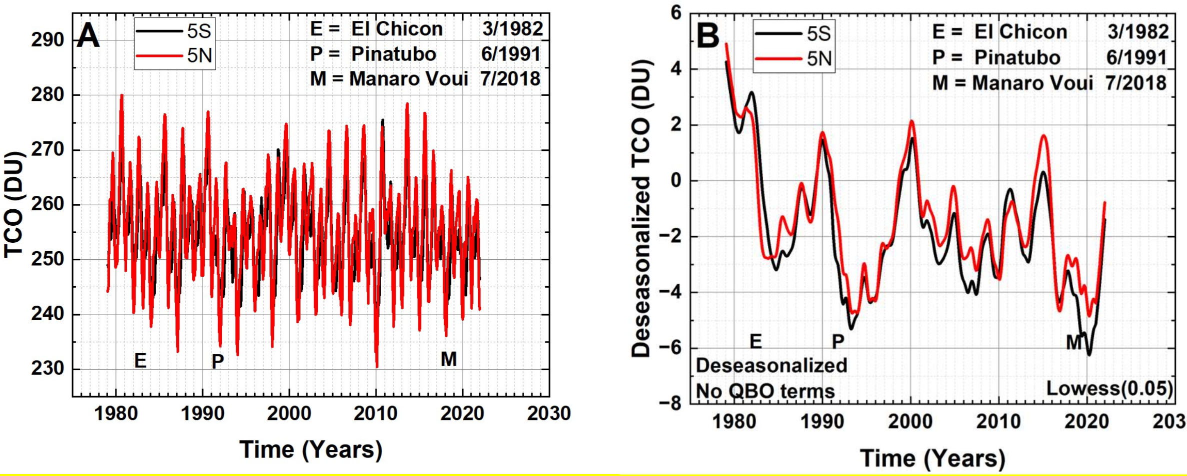

Fig. 4. A. Ω_{MOD} time series for θ = 5°N and 5°S. B. The deseasonalized TCO time series for θ = 5°N and 5°S without removing QBO effects (Eq. 1). The approximate dates are shown of volcanic eruptions that injected large amounts of SO_2 into the stratosphere leading to minima approximately 1 year later.

Figure 4A shows the Ω_{MOD} time series for 5^{O}S and 5^{O}N, and Fig. 4B the deseasonalized and smoothed (Lowess(0.05)) Ω_{MOD} time series. After deseasonalizing, but not removing QBO effects (Eq. 1), both the 2.3-year QBO oscillation and the reduced ozone effects from volcanic eruptions, are shown in Fig. 4B. Some volcanos (e.g., from El Chicon March 1982, Mt. Pinatubo June 1991, and Manaro Voui July 2018) inject significant amounts of SO_2 into the lower stratosphere leading to the formation of aerosols that reduce UV light and the production of ozone, especially in the equatorial region.

Figure 5 shows the Lowess(0.3) fits (black curves) to the Ω_{MOD} data for four sample latitude bands 55^{O}S, 45^{O}S, 55^{O}N, and 45^{O}N that tracks the longer-term changes in the Ω_{MOD} time series. Also shown are examples of f = 0.1 (red) and f = 0.05 (blue dots). The Lowess(0.05) fit (blue dots) shows considerable structure with a minimum in 1993 that is likely related to the Mt. Pinatubo eruption and a modest El Nino effect in 1991-1992. The estimated values of T_A for f = 0.1 and 0.05 can differ by 6 months from that determined when f=0.3 because of short term oscillations. The Lowess(0.3) degree of smoothing removes most of the short-term effects on ozone such as QBO and those from volcanic eruptions from El Chichon (1982) and Mt. Pinatubo (1991), both well before the earliest estimated T_A in 1994.

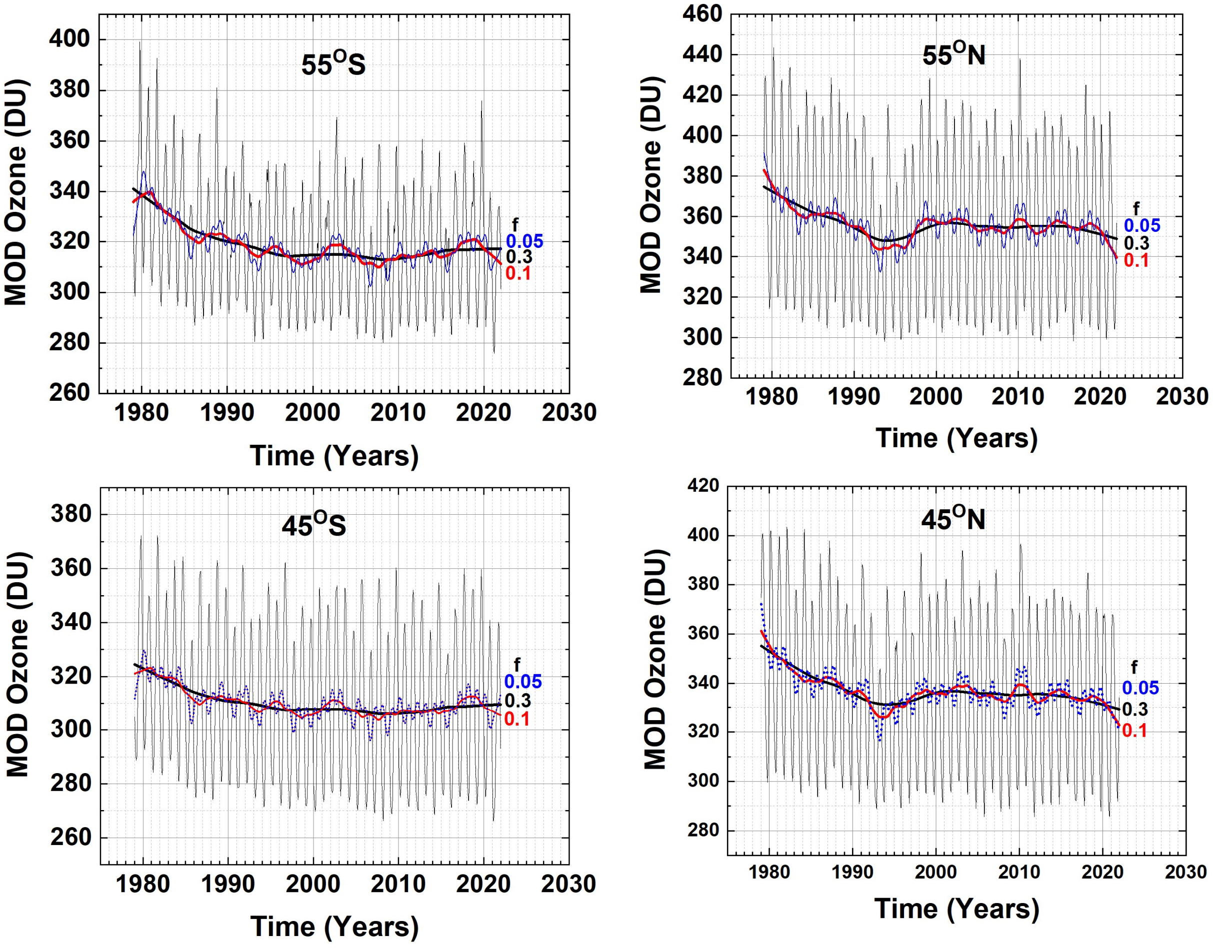

Fig. 5 Ω_{MOD} in four latitude bands and Lowess(0.3) fitting functions (f = 0.3, black lines). Examples of different f = 0.1 (Red) and 0.05 (blue dots) are shown at 45^{O}S and 45^{O}N. Note the slight downturn since 2010 in the Lowess(0.3) at 45^{O}N and 55^{O}N.

Figure 6 shows the Lowess(0.3) fits to the Ω_{MOD} data (1979 to 2021) for 16 latitude bands, $-75^O < \theta < 75^O$ on an expanded ozone scale. Each of the Lowess(0.3) plots for the various latitudes shows different periods of ozone decrease and subsequent turnaround $T_A(\theta)$ after the mid-1990's. Use of expanded ozone scales appears to show a sharp downturn after 2010 at some latitudes (25^ON to 75^ON). As shown later, the apparent downturns in the Lowess(0.3) fit to Ω_{MOD} after 2010 are not yet statistically significant in trend estimates from Ω_{MOD} as an indicator of long-term ozone decrease.

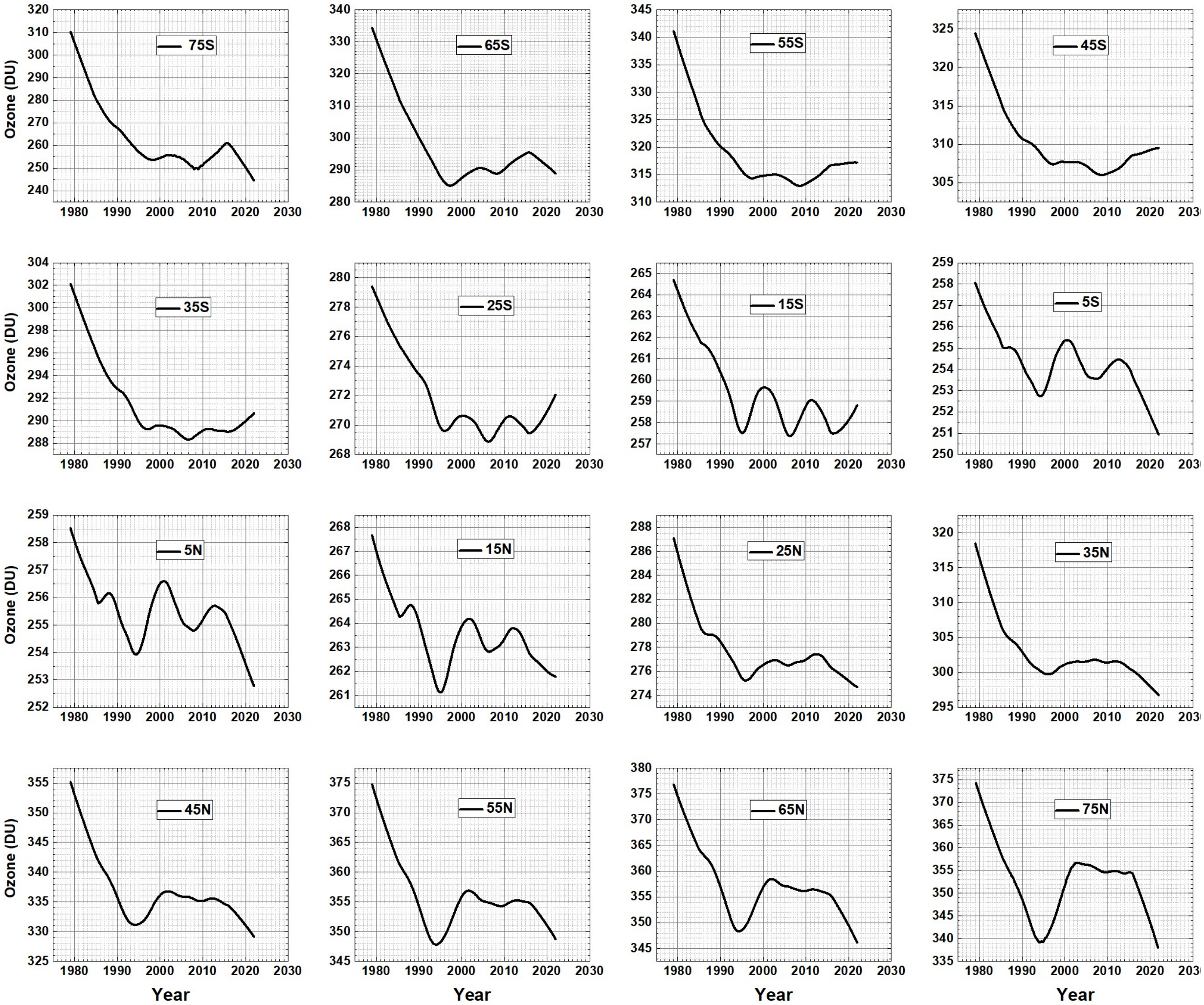

Fig. 6 Lowess(0.3) fits to the Ω_{MOD} data for 16 latitude bands used to determine $T_A(\theta)$. Note that the ozone scale varies for each latitude.

Figure 7 shows the turnaround dates $T_A(\theta)$ that are obtained by taking the 1st derivatives of Fig. 6 data and finding the zero-crossing time corresponding to the appropriate minimum value in Fig. 6. The exact turnaround dates determined have a precision of ±0.1 years and an accuracy of ±0.5 years. The ±0.5 uncertainty does not affect the calculation of trends before and after the estimated $T_A(\theta)$. What is interesting is that some of the turnaround dates in Fig. 7 are separated by over 4 years and are strongly asymmetric between the hemispheres. Figure 7 shows a near symmetry for early turnaround dates

1994-1996 for low latitudes between ±25^{O} that corresponds to the Brewer-Dobson ozone upwelling region (Brewer et al., 1926; Dobson, 1949; Butchart, 2014) where most of the ozone is created by sunlight and then transported poleward. At poleward latitudes, the turnaround dates are quite different, with a delayed date, 1997, at high SH latitudes (35^{O}S – 65^{O}S), 1998 at 75^{O}S compared to 1994 at high NH latitudes (45^{O}N to 75^{O}N).

The T_A delay to 1997 for latitudes 35^{O}S – 65^{O}S follows the delayed recovery of ozone depletion within the Spring Antarctic Ozone Hole (Solomon, 1990; Stone et al., 2021, their Fig. 3; Bodeker and Kremser, 2021, their Figs. 6 and 9) and backfilling (air exchange with lower latitude ozone-rich air) during the summer months after the polar vortex winds break down in October – November.

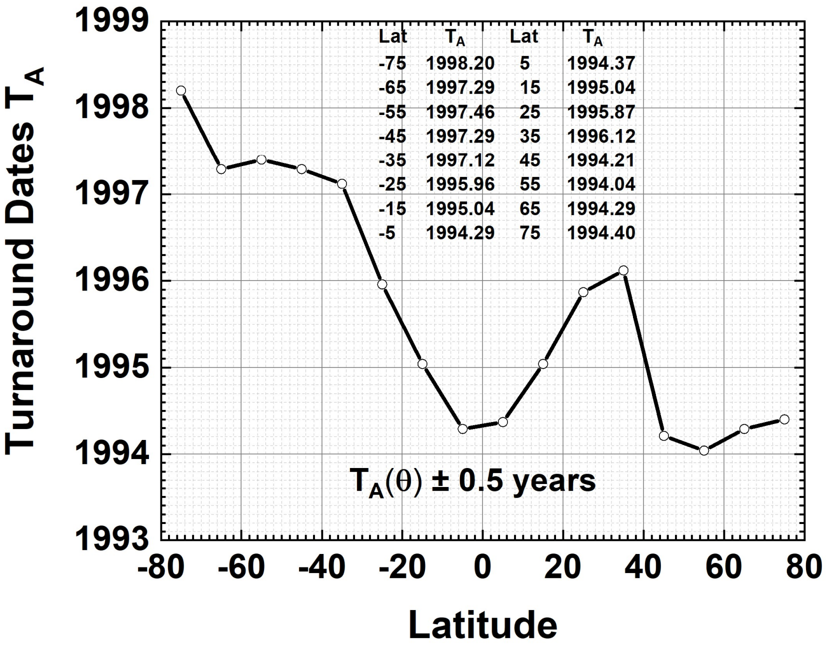

Fig 7 Turnaround dates $T_A(\theta)$ as a function of latitude from Fig.6 with an estimated accuracy of ±0.5 years based on the analysis in Fig. 5.

The general $T_A(\theta)$ pattern shown in Fig. 7 should appear in model calculations as a signature of the combined effects of photochemistry, dynamics, and volcanic eruptions on the cessation of decreasing ozone in the mid-1990s.

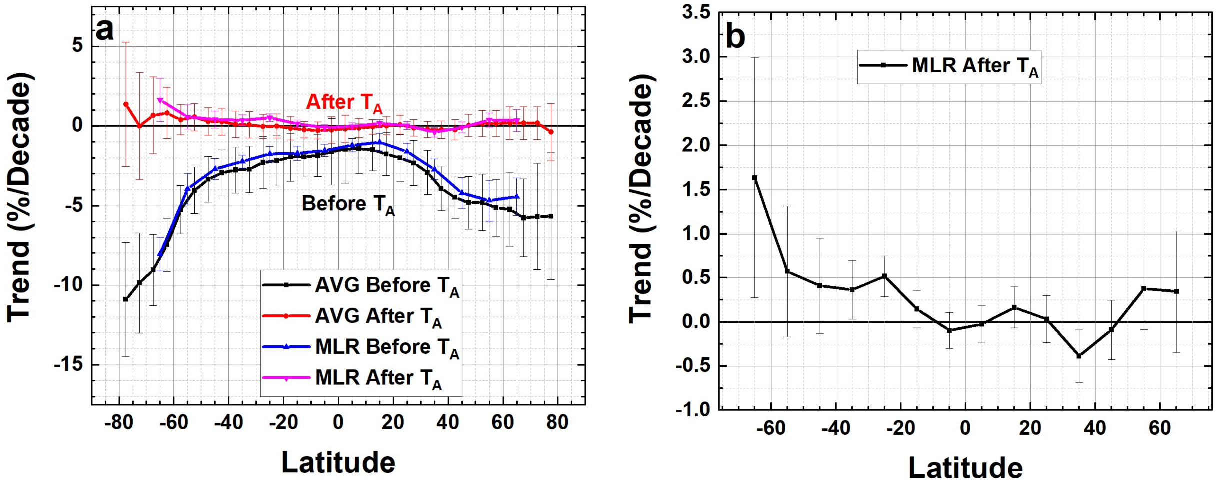

Fig. 8a Ozone trends $P_D(\theta)$ (percent per decade) using the MLR and Annual Average methods before and after $T_A(\theta)$. 6b A magnified version of the MLR estimated trends after T_A with 2σ uncertainties.

Trends (linear slopes) $P_D(\theta)$ in percent per decade are estimated (Eqn. 3) for the separate periods before and after $T_A(\theta)$ in each latitude band (Fig. 8) and for the entire period (Fig. 3). The linear slopes obtained by the two methods, MLR and annual average closely agree (Figs. 3 and 8) with the annual average method extended to polar latitudes (Fig. 8a). Table 1 contains the data from Figs. 8a and 8b.

Table 1 MLR Trends (%/decade) ± 2σ

Latitude	P_D Before T_A	P_D After T_A
-65	-8.04±1.1	1.64±1.4
-55	-3.93±1.0	0.57±0.7
-45	-2.69±0.7	0.41±0.5
-35	-2.22±0.4	0.36±0.3
-25	-1.75±0.5	0.52±0.2
-15	-1.71±0.4	0.15±0.2
-5	-1.54±0.4	-0.10±0.2
5	-1.21±0.4	-0.03±0.2
15	-1.01±0.6	0.16±0.2
25	-1.61±0.5	0.03±0.3
35	-2.71±0.6	-0.39±0.3
45	-4.20±1.0	-0.09±0.3
55	-4.67±1.3	0.38±0.5
65	-4.43±1.2	0.35±0.7

The latitude dependent trends derived by Weber et al. (2022) using 1996.5 as the approximate T_A (their Fig. 3) agree within error bars with the trends shown in Fig. 8 for all latitudes but they suggest T_A = 2000 for the polar regions. The trends also agree within error bars with those in WMO (2022). As mentioned earlier, the trend estimates are not very sensitive to the exact T_A, but the shape of $T_A(\theta)$ should be a model validation marker contained in model calculations for all effects, not just ODSs.

The delayed (1997) Southern Hemisphere mid and high latitude values of T_A are caused by coupling to the increasing Antarctic spring ozone loss after 1979 until a recovery starting in about 1998-2000 (Solomon et al., 2016). The mid and high latitude, from 35°S to 65°S, delay is caused by the summer mixing of ozone poor air from the Antarctic region with SH midlatitude ozone-rich air once the polar vortex winds break down in November-December.

The asymmetry between the Arctic and Antarctic is caused by the lower winter Antarctic temperatures (-80°C) leading to the formation of low altitude clouds containing ice crystals along with the isolating Antarctic polar vortex winds (Solomon et al., 2007; 2016). In the spring sunlight the ice and water droplets (Tritscher, et al., 2021) release ODS and depletes ozone to a monthly average of about 155 DU. During the summer, air exchange with ozone rich air from lower latitudes comes into the polar latitudes and fill in the ozone layer above Antarctica (monthly average about 300 DU. Smaller but significant ozone losses occurred in the Artic region caused by occasional low temperatures and ODSs. The Arctic does not routinely have the low temperatures needed for winter ice clouds nor does it have the persistent isolating polar vortex winds because of wave action forced by the land topography The latitude band at 75°N (Fig.1) has the highest amount of monthly average winter ozone 450±25 DU that decreases to 290±20 DU monthly average during the summer that are comparable to mid-latitude values. The result is earlier values of T_A in the NH compared to the SH. The NH T_A is earlier than the 1997 minimum in stratospheric halogens (Weber et al., 2022; Newman et al., 2007). Note that T_A is not the time of the start of recovery, but rather the time for the end of rapid ozone decrease.

Before the SH T_A, total column ozone decreased at a rate of P_D= -10.9±3.6% at 77.5°S and -8.0±1.1% per decade at 65°S, during the period from 1979 to 1997 with smaller decreases from 55°S to 25°S (Fig. 8a). After the turnaround period T_A, ozone at 65°S increased at P_D = 1.6±1.4%/decade based on the MLR method. After T_A, most other latitudes (Fig. 8b) show stationary ozone amounts within 2σ. In the NH the decreases were smaller than in the SH before T_A because of the absence of an Arctic ozone hole region. At 77.5°N was P_D = -5.6±4%/decade and at 65°N P_D = -4.4±0.35 %/decade.

An analysis of ozone trends prior to the start of reliable satellite data in late 1978 showed that the annual rate of ozone loss (%/Year) increased after 1978 (Staehelin et al., 2001). Based on the first derivatives of the data in Fig. 6, the maximum annual rate of ozone reduction occurred in 1979 and 1980 in the NH and SH (Fig. 9) except for 65°N in 1992 where the rate of loss is -8.75%/Year. The loss rates range from -20.6 %/Year at 75°S to 2.39 %/Year at 5°N. A smaller loss rate occurred for 35°N to 75°N where the loss rate is almost constant between 8%/Year and 10%/Year compared to the larger SH loss rates caused by the presence of the springtime Antarctic ozone hole.

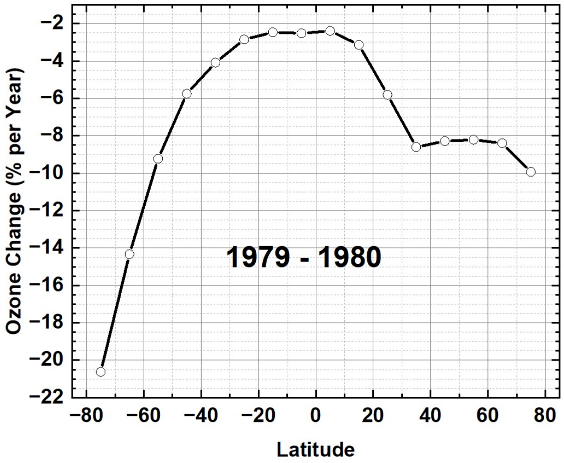

Fig. 9 The percent change in ozone per year in 1979 or 1980

The Lowess(0.3) plots in Fig. 6 suggest that Ω_{MOD} has been declining since approximately 2010 from 5^OS to 65^ON but still increasing from 45^OS to 65^OS (Fig. 6). However, computing the trends (Fig. 10) from $\Omega_{MOD}(t,\theta)$ using either the MLR (Eq. 1) or annual average methods suggest that the declines in ozone from 25^OS to 65^ON are not yet significant at the 2σ level over the period 2010 – 2021.

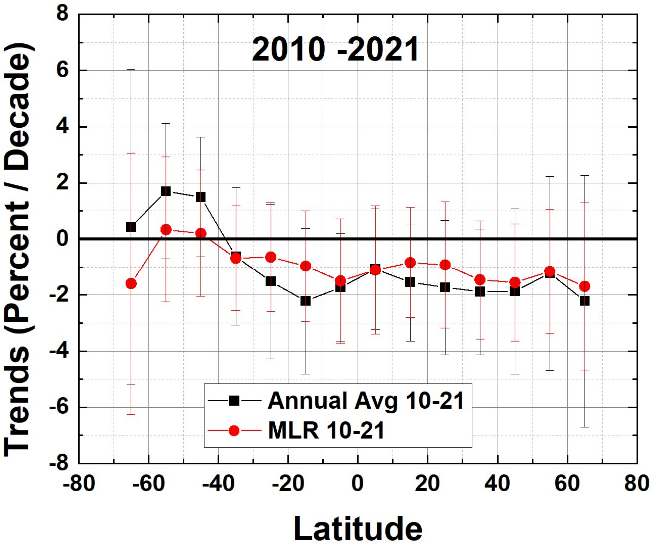

Fig. 10 Ozone trends $P_D(\theta)$ (Percent per Decade) for the period 2010 – 2021 for the Annual Average and MLR methods applied to $\Omega_{MOD}(t,\theta)$.

Comparing deseasonalized $\Omega_{MOD}(t,\theta)$ with deseasonalized Microwave Limb Sounder MLS (see Appendix Figs. A1, A2, and A3) Stratospheric Ozone from 2005 to 2021 shows small average (Lowess(0.3)) differences that are within ±1DU except for 2021 when the differences at both 65^OS and 65^ON are about -2.5DU. This suggests that the calibrations of the later SBUV-2 and OMPS-NP instruments are stable. For

2016 to 2018, Ω_{MOD} is obtained from NOAA-19 SBUV plus OMPS-NP and from just OMPS-NP since 2018. Figure A3 suggests that there was a decrease in tropospheric ozone in 2020 that may correspond to reduced economic activity during the COVID-19 pandemic.

Age of air AoA is a measure of how long a parcel of air resides in the stratosphere after it leaves the troposphere (Linz et al., 2016; Ploeger et al, 2021). A comparison of T_A with AoA estimates from the relatively inert tracer gas CO_2 (Fig. 11) for the altitude range near the ozone maximum (approximately 20 km) vs latitude (based on Waugh and Hall, 2002, their Fig. 6a and Ploeger et al, 2021 their Fig. 10a) shows near symmetry between the hemispheres with the shortest AoA in the equatorial region. The turnaround dates T_A in Fig. 6 are also symmetric in the equatorial zone corresponding the upwelling Brewer Dobson circulation and the smaller AoA. This suggests that the combined effects of chemistry and dynamics on ozone amounts are similar between $\pm 25^{O}$. The precursors to ODS are also lifted into the equatorial stratosphere and transported towards the polar regions (Newman et al., 2004; 2007) where they can be photo-dissociated into ODS. Ozone at higher latitudes, NH and SH, with longer AoA, will be dependent on transported ozone and ODS and their photochemistry, and especially the different dynamics and chemistry in the Arctic and Antarctic regions.

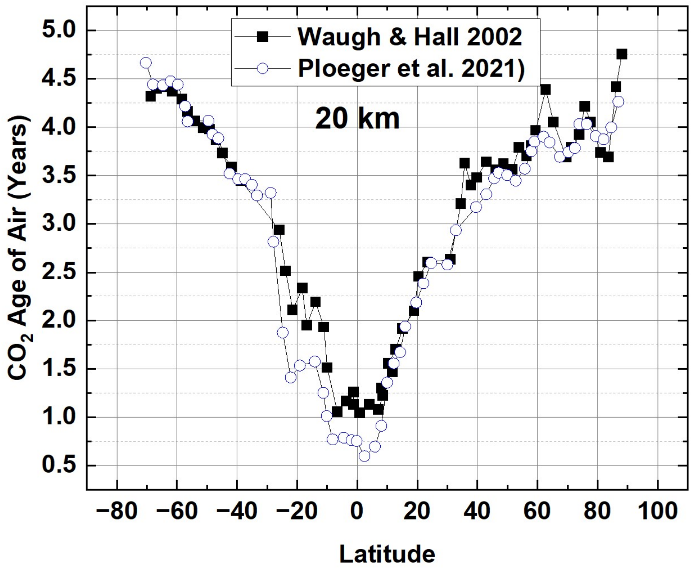

Fig. 11 Age of air derived from CO_2 data (Waugh and Hall, 2002; Ploeger et al., 2021)

3.0 Summary

The monthly averaged Merged Ozone Data set Ω_{MOD} (2.5^O latitude bands, 77.5^OS to 77.5^ON) from 1979 to 2021 were averaged into 10^O latitude bands $75^O\text{S} < \theta < 75^O\text{N}$. A smoothed Ω_{MOD} version based on Lowess(0.3) was used to determine the approximate dates of the latitude dependent ozone end of ozone decrease date $T_A(\theta)$ ranging from 1994 to 1998 with an error estimate of ±0.5 years. The systematic hemispherically asymmetric latitude dependent pattern $T_A(\theta)$ should appear in atmospheric models that combine the effects of volcanic eruptions, photochemistry, and dynamics in their estimate of the end of ozone decrease. The hemispheric asymmetry is caused by the formation of the annual Spring Antarctic ozone (monthly spring average about 155 DU) hole with persistent isolating polar vortex winds followed by the summer mixing with mid-latitude ozone rich air (December average about 300 DU). The Arctic region does not form a large spring ozone hole, nor does it have sustained isolating polar vortex winds. Instead at 75^ON (Fig. 1) it has the highest amount of monthly average winter ozone 450±25 DU that decreases to 290±20 DU monthly average during the summer. Trends of ozone $P_D(\theta)$ in percent per decade were computed before and after the latitude dependent $T_A(\theta)$ using two different methods, MLR and annual averages, that closely agree over their mutual latitude range of validity, 65^OS to 65^ON. The annual average method can extend into polar latitudes. The most dramatic rates of ozone loss were $P_D = -10.9\pm3.6\%$ decade at 77.5^OS and -8.0±1.1%/decade at 65^OS, which is about double the rate of loss of $P_D = -5.7\pm4$ %/decade at 77.5^ON and -4.4±1.2% per decade at 65^ON. During the period after T_A to 2021, there has been a small increase at latitudes in the SH from 25^OS to 65^OS with the largest value being 1.6±1.4% per decade at 65^OS. Aside from the small increases in the SH region there has been no statistically significant ozone recovery toward 1979 values, just an almost constant ozone amount after $T_A(\theta)$. The largest annual rate of ozone decrease occurred near the beginning of the SBUV data record, 1979, showing large high latitude losses of -20.6 %/Year at 75^OS caused by the springtime Antarctic ozone hole compared to a smaller Arctic loss of -9.9%/Year at 75^ON. During the period 2010 to 2021, there has been a small apparent decrease in ozone amount in Ω_{MOD} that is not yet statistically significant at the 2-standard deviation level. A comparison between Ω_{MOD} and MLS stratospheric column ozone shows small systematic negative differences in 2020 that mostly recovered in 2021 except near the equator. This suggests that there is no statistically significant instrumental calibration drift between Ω_{MOD} TCO and MLS stratospheric ozone.

Appendix

The MOD TCO data record since 2018 is obtained from OMPS-NP, which appears to show decreasing TCO (Fig. 6). Because of this, the deseasonalized Ω_{MOD} are compared with MLS (Microwave Limb Sounder) deseasonalized stratospheric column ozone for the period 2004 to 2021 to look for calibration drifts in the Ω_{MOD} time series. The question addressed here is not the absolute agreement between Ω_{MOD} and the MLS mostly stratospheric ozone column, but rather if there is a systematic drift between the two data sets after 2016. Figures A1 and A2 show that the difference between the two deseasonalized time series for latitudes from 65°S to 65°N and for the entire period 2005 – 2021. Of interest is the period 2016 to 2021 when Ω_{MOD} was derived using NOAA-19 SBUV plus OMPS-NP 2016 – 2018 and from OMPS-NP since 2018.

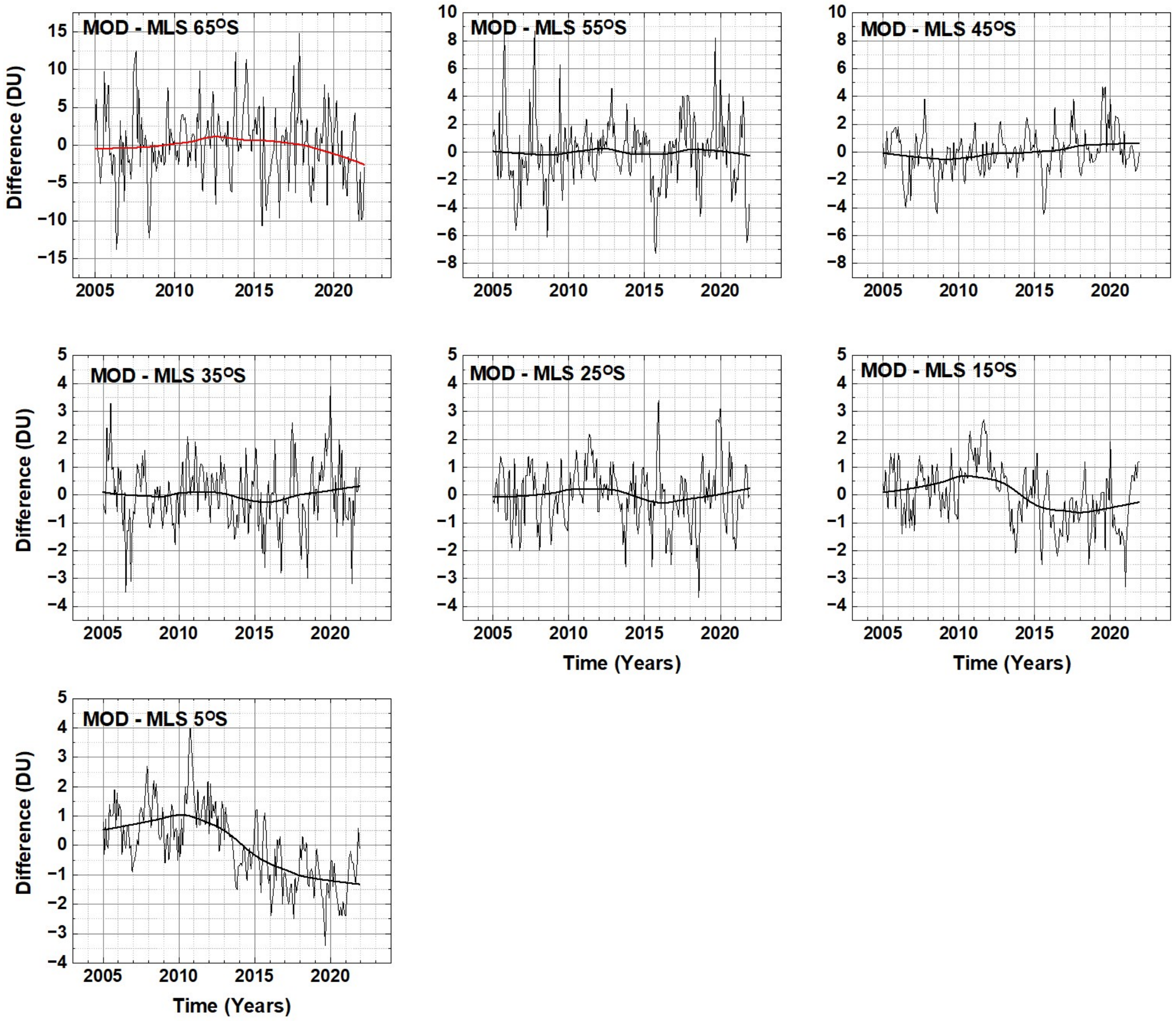

Fig. A1 A comparison of deseasonalized Ω_{MOD} with deseasonalized MLS stratospheric column ozone for 65°S to 5°S.

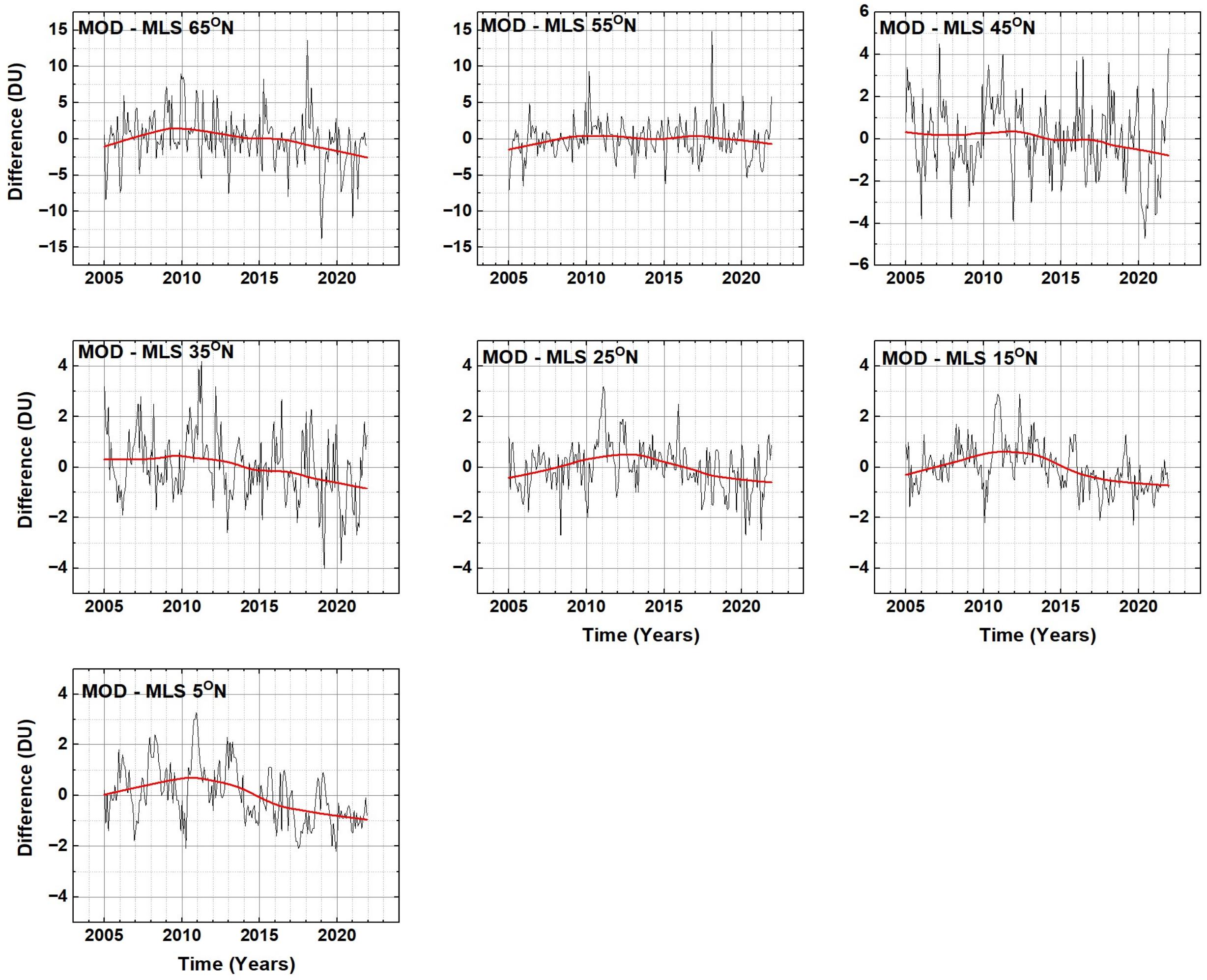

Fig. A2 A comparison of deseasonalized MOD total ozone with deseasonalized MLS stratospheric column ozone for 5^{O}N to 65^{O}N. Variations of ±3DU are within the MOD merged record uncertainties.

The differences in Figs A1 and A2 between Ω_{MOD} and MLS since 2016 are not statistically significant at the 2σ level. Variations of ± 3DU are within the Ω_{MOD} merged record uncertainties.

Since both MOD and MLS time series were deseasonalized, the mean values would be zero unless there were changes in tropospheric ozone or instrument calibration drift. The differences are summarized in Fig. A3 along with the $2\sigma'$, (σ' = standard deviation from the mean) error bars estimated from the average of each deseasonalized time series. In 2020 there appears to be a systematic change in <MOD – MLS> that may be a reduction in tropospheric ozone amount of about 3 DU caused by the economic slowdown associated with COVID-19 (Ziemke et al, 2022). The systematic change mostly recovered in 2021 (Fig. A3) except for -1DU near the equator (-5^{O}S to 15^{O}N).

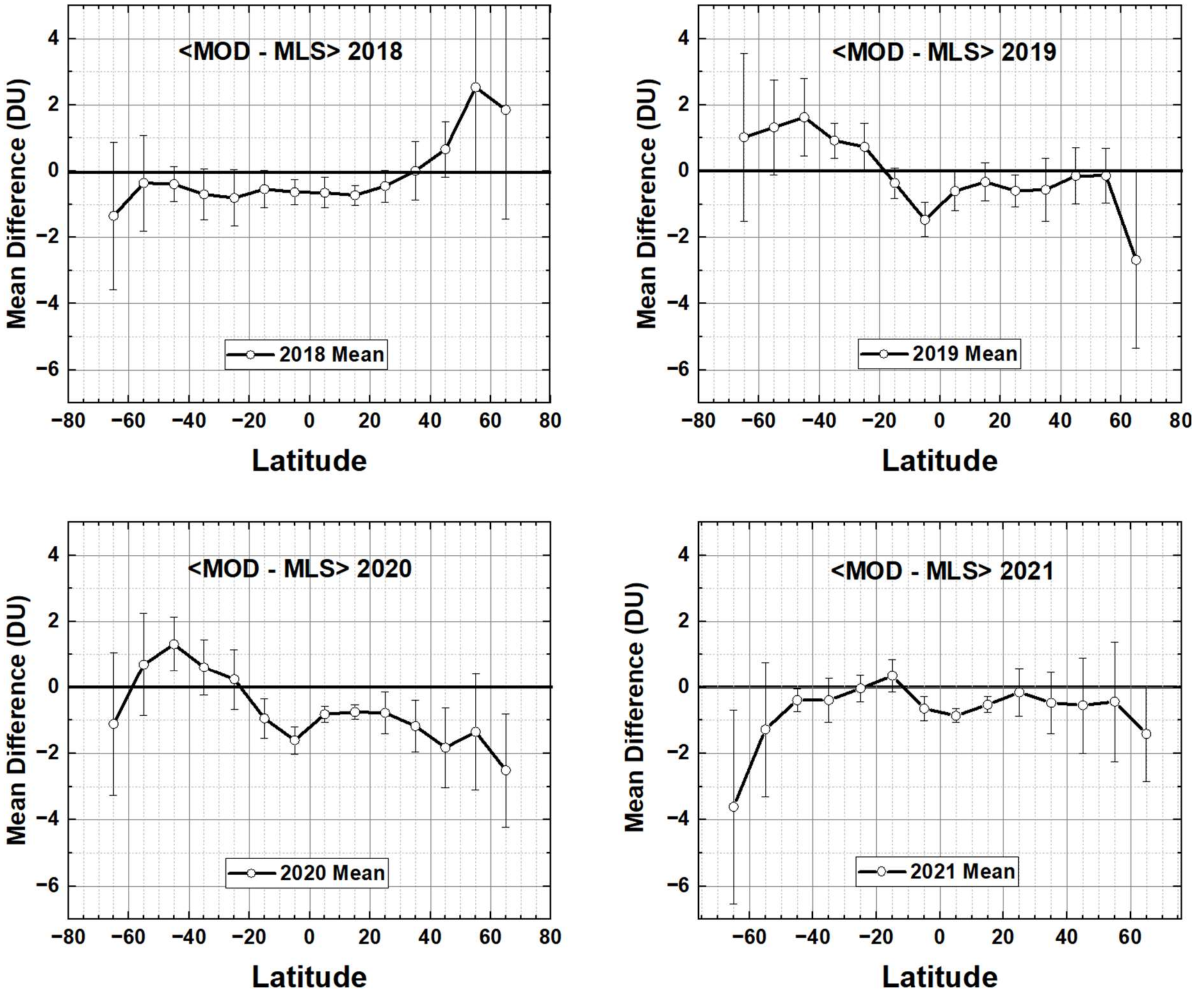

Fig. A3 Annual average <MOD – MLS> for the years 2018 to 2021. Error bars are 2σ’, where σ’ = standard error of the mean estimated from the average of the deseasonalized time series for each year shown in Figs. A1 and A2.

4.0 References

Bai, K., N.-B. Chang, R. Shi, H. Yu, and W. Gao, An intercomparison of multidecadal observational and reanalysis data sets for global total ozone trends and variability analysis, J. Geophys. Res. Atmos., 122, 7119–7139, doi:10.1002/2016JD025835, 2017.

Bhartia, P. K. , R. D. McPeters, L. E. Flynn, S. Taylor, N. A. Kramarova, S. Frith, B. Fisher, and M. DeLand, Solar Backscatter UV (SBUV) total ozone and profile algorithm. Atmos. Meas. Tech., 6, 2533–2548, doi:10.5194/amt-6-2533-2013, 2013.

Bodeker, G. E. and Kremser, S.: Indicators of Antarctic ozone depletion: 1979 to 2019, Atmos. Chem. Phys., 21, 5289–5300, https://doi.org/10.5194/acp-21-5289-2021, 2021.

Brewer, A. W., Evidence for a world circulation provided by the measurements of helium and water vapour distribution in the stratosphere, Quarterly Journal of the Royal Meteorological Society. 75 (326): 351–363. Bibcode:1949QJRMS..75..351B. doi:10.1002/qj.49707532603. ISSN 1477-870X, 1949.

Crutzen, P. J. and Arnold, F.: Nitric acid cloud formation in the cold Antarctic stratosphere: a major cause for the springtime “ozone hole”, Nature, 342, 651–655, https://doi.org/10.1038/324651a0, 1986.

Dameris, Martin and Mark P. Baldwin, Impact of Climate Change on the Stratospheric Ozone Layer, Stratospheric Ozone Depletion and Climate Change, Edited by Rolf Muller, Chapter 8, 214-252, Royal Society of Chemistry 2012.

Dobson, G. M. B.; Harrison, D. N.; Lindemann, F. A., Measurements of the amount of ozone in the Earth's atmosphere and its relation to other geophysical conditions, Proceedings of the Royal Society of London. Series A, Containing Papers of a Mathematical and Physical Character. 110 (756): 660–693. Bibcode:1926RSPSA.110..660D. doi:10.1098/rspa.1926.0040. 1926.

Butchart, N., The Brewer-Dobson circulation, Rev. Geophys.,52, 157–184, doi:10.1002/2013RG000448, 2014.

Cleveland, W.S., Robust Locally Weighted Regression and Smoothing Scatterplots, Journal of the American Statistical Association, Vol. 74, pp. 829-836, https://doi.org/10.2307/2286407, 1979.

Cleveland, W.S. and Devlin, S.J., Locally Weighted Regression: An Approach to Regression Analysis by Local Fitting," Journal of the American Statistical Association, Vol. 83, pp. 596-610, DOI: 10.1080/01621459.1988.10478639 1988.

DeLand, M. T., S. L. Taylor, L. K.Huang, and B. L. Fisher, Calibration of the SBUV version 8.6 ozone data product, Atmos. Meas. Tech., 5, 2951–2967, doi:10.5194/amt-5-2951-2012, 2012.

Frith, S. M., N. A. Kramarova, R. S. Stolarski, R. D. McPeters, P. K. Bhartia, and G. J. Labow, Recent changes in total column ozone based on the SBUV Version 8.6 Merged Ozone Data Set, J. Geophys. Res. Atmos., 119, 9735-9751, doi:10.1002/2014JD021889, 2014.

Frith, S. M., Stolarski, R. S., Kramarova, N. A., and McPeters, R. D.: Estimating uncertainties in the SBUV Version 8.6 merged profile ozone data set, Atmos. Chem. Phys., 17, 14695–14707, https://doi.org/10.5194/acp-17-14695-2017, 2017.

Frith, S. M., Bhartia, P. K., Oman, L. D., Kramarova, N. A., McPeters, R. D., and Labow, G. J.: Model-based climatology of diurnal variability in stratospheric ozone as a data analysis tool, Atmos. Meas. Tech., 13, 2733-2749, https://doi.org/10.5194/amt-13-2733-2020, 2020.

Guttman, I., Linear Models, An Introduction, 358 pp., Wiley-Interscience, New York, 1982.

Herman, J.R., R. McPeters, D. Larko, Ozone depletion at northern and southern latitudes derived from January 1979 to December 1991 Total Ozone Mapping Spectrometer data, 98, 13783-12793 https://doi.org/10.1029/93JD00601, 1993.

Khosrawi, F., Urban, J., Pitts, M. C., Voelger, P., Achtert, P., Kaphlanov, M., Santee, M. L., Manney, G. L., Murtagh, D., and Fricke, K.-H.: Denitrification and polar stratospheric cloud formation during the Arctic winter 2009/2010, Atmos. Chem. Phys., 11, 8471–8487, https://doi.org/10.5194/acp-11-8471-2011, 2011.

Linz, Marianna, R. Alan Plumb, Edwin P. Gerber, Aditi Sheshadri, The Relationship between Age of Air and the Diabatic Circulation of the Stratosphere. J. Atmos. Sci., 73, 4507-4518, doi: 10.1175/JAS-D-16-0125.1, 2016.

McPeters, R. D., P. K. Bhartia, D. Haffner, G. J. Labow, and L. Flynn, The version 8.6 SBUV ozone data record: An overview, J. Geophys. Res. Atmos., 118, 8032-8039, doi:10.1002/jgrd.50597., 2013.

Newman, P.A., S. R. Kawa, E. R. Nash, On the size of the Antarctic ozone hole, Geophys. Res. Lett., 1-4, 31, doi:10.1029/2004GL020596, 2004.

Newman, P. A., Daniel, J. S., Waugh, D. W., and Nash, E. R., A new formulation of equivalent effective stratospheric chlorine (EESC), Atmos. Chem. Phys., 7, 4537–4552, https://doi.org/10.5194/acp-7-4537-2007, 2007.

Oldenborgh, Geert Jan van, Harry Hendon, Timothy Stockdale, Michelle L'Heureux, Erin Coughlan de Perez, Roop Singh, and Maarten van Aalst, Defining El Niño indices in a warming climate, Environ. Res. Lett. 16 044003, DOI 10.1088/1748-9326/abe9ed, 2021.

Randel, W. J., and J. B. Cobb, Coherent variations of monthly mean total ozone and lower stratospheric temperature, J. Geophys. Res., 99, 5433--5447, DOI:10.1029/93JD03454, 1994.

Solomon, S., Garcia, R. R., Rowland, F. S., and Wuebbles, D. J.: On the depletion of Antarctic ozone, Nature, 321, 755–758, https://doi.org/10.1038/321755a0, 1986.

Solomon, S., Stratospheric ozone depletion: a review of concepts and history, Rev. Geophys., 37, 275–316, https://doi.org/10.1029/1999RG900008, 1999.

Solomon, S., Portmann, R. W., & Thompson, D. W., Contrasts between Antarctic and Arctic ozone depletion. Proceedings of the National Academy of Sciences, 104(2), 445-449. https://doi.org/10.1073/pnas.0604895104, 2007.

Solomon, Susan, Diane J. Ivy, Doug Kinnison, Michael J. Mills, Ryan R. Neely, Iii, And Anja Schmidt, Emergence of healing in the Antarctic ozone layer, Vol 353, 269-274 DOI: 10.1126/science.aae0061, 2016.

Staehelin, J., N. Harris, C. Appenzeller, and J. Eberhard, Ozone trends: A review, REV GEOPHYS., 39,231-290, 10.1029/1999RG000059, 2001.

Stolarski R. D., P. Bloomfield, R. D. McPeters, and J. R. Herman, Total ozone trends deduced from Nimbus 7 TOMS data, Geophys., Res., Lett., 18, https://doi.org/10.1029/91GL01302, 1991.

Stolarski R, Bojkov R, Bishop L, Zerefos C, Staehelin J, Zawodny J. Measured trends in stratospheric ozone, Science, Apr 17;256(5055):342-9. doi: 10.1126/science.256.5055.342. PMID: 17743110, 1992.

Stone, K. A., Solomon, S., and Kinnison, D. E., On the identification of ozone recovery. Geophysical Research Letters, 45, https://doi.org/10.1029/2018GL077955, 2018.

Stone KA, Solomon S, Kinnison DE, Mills MJ. On Recent Large Antarctic Ozone Holes and Ozone Recovery Metrics. Geophys Res Lett. 2021 Nov 28;48(22):e2021GL095232. doi: 10.1029/2021GL095232. Epub 2021 Nov 18. PMID: 35864979; PMCID: PMC9286815.

Strahan, S. E., and Douglass, A. R., Decline in Antarctic ozone depletion and lower stratospheric chlorine determined from Aura Microwave Limb Sounder observations. Geophysical Research Letters, 45, 382–390. https://doi.org/10.1002/2017GL074830, 2018.

Tritscher, I., Pitts, M. C., Poole, L. R.,Alexander, S. P., Cairo, F., Chipperfield, M. P., et al. (2021). Polar stratospheric clouds: Satellite observations, processes, and role in ozone depletion. Reviews of Geophysics, 59, e2020RG000702. https://doi.org/10.1029/2020RG000702, 2021.

Velders, G. J., & Andersen, S. O. (2018). The Montreal Protocol on Substances that Deplete the Ozone Layer and its amendments: An overview. Air Pollution and Health, 11-28, 2018.

Wallace, J. M., R. L. Panetta, and J. Estberg, Representation of the equatorial stratospheric quasi-biennial oscillation in EOF phase space, J. Atmos. Sci., 50, 1751--1762, https://doi.org/10.1175/1520-0469(1993)050<1751:ROTESQ>2.0.CO;2, 1993.

Weatherhead, E. C., Reinsel, G. C., Tiao, G. C., Meng, X.-L., Choi, D., Cheang, W.-K., Keller, T., DeLuisi, J., Wuebbles, D. J., Kerr, J. B., Miller, A. J., Oltmans, S. J., and Frederick, J. E.: Factors affecting the detection of trends: Statistical considerations and applications to environmental data, 103,17149–17161, https://doi.org/10.1029/98JD00995, 1998.

Waugh, D.W. and Hall, T.M., Age of stratospheric air: theory, observations, and models, Rev. of Geophys., 40,1-10, doi:10.1029/2000RG000101, 2002.

Weber, Mark, Carlo Arosio, Melanie Coldewey-Egbers, Vitali E. Fioletov, Stacey M. Frith, Jeannette D. Wild, Kleareti Tourpali, John P. Burrows, and Diego Loyola, Global total ozone recovery trends attributed to ozone-depleting substance (ODS) changes derived from five merged ozone datasets, https://doi.org/10.5194/acp-22-6843-2022, ACP, 22, 6843–6859, 2022.

World Meteorological Organization (WMO), Scientific Assessment of Ozone Depletion: 2022, GAW Report No. 278, 509 pp., WMO, Geneva, 2022.

Ziemke, Jerry R. Luke D. Oman, Sarah A. Strode, Anne R. Douglass, Mark A. Olsen, Richard D. McPeters, Pawan K. Bhartia, Lucien Froidevaux, Gordon J. Labow, Jacquie C. Witte, Anne M. Thompson, David P. Haffner, Natalya A. Kramarova, Stacey M. Frith, Liang-Kang Huang, Glen R. Jaross, Colin J. Seftor, Mathew T. Deland, Steven L. Taylor, Trends in global tropospheric ozone inferred from a composite record of TOMS/OMI/MLS/OMPS satellite measurements and the MERRA-2 GMI simulation, Atmospheric Chemistry and Physics, 10.5194/acp-19-3257-2019, **19**, 5, (3257-3269), 2019.

Ziemke, J. R., N. A. Kramarova, S. M. Frith, L.-K. Huang, D. P. Haffner, K. Wargan, L. N. Lamsal, G. J. Labow, R. D. McPeters, and P. K. Bhartia, NASA satellite measurements show global-scale reductions in tropospheric ozone in 2020 and again in 2021 during COVID-19, Geophys. Res. Lett., 49, https://doi.org/10.1029/2022GL098712, 2022.

Author contribution:

Jay Herman is responsible for writing the text, the annual integral trend calculations, and all the figures. Jerald Ziemke supplied the MLR trend calculations and the comparison with MLS. Richard McPeters supplied the MOD ozone as a continuous function of time from 1979 to 2021 for each latitude band.

Data Availability

The original data used are publicly available in an ASCII format.

https://acd-ext.gsfc.nasa.gov/Data_services/merged/

and processed data in Excel format

https://avdc.gsfc.nasa.gov/pub/DSCOVR/JayHerman/MOD_Ozone_Trends/

Competing interests:

The authors declare that they have no conflict of interest.

Acknowledgements:

The authors want to acknowledge the contribution and help of Stacey Frith for compiling the SBUV and OMPS-NP data sets to produce the long ozone data record. She also reviewed the paper and added some important corrections.